Grating-coupled transmission-type surface plasmon resonance sensors based on dielectric and metallic gratings

Kyung Min Byun,[1] Sung June Kim,[1] and Donghyun Kim[2,*]

[1]School of Electrical Engineering and Computer Science, Seoul National University, Seoul 151-742, South Korea
[2]School of Electrical and Electronic Engineering, Yonsei University, Seoul 120-749, South Korea

*Corresponding author: kimd@yonsei.ac.kr

Received 29 March 2007; accepted 24 May 2007;
posted 4 June 2007 (Doc. ID 81601); published 8 August 2007

We investigated grating-coupled transmission-type surface plasmon resonance (SPR) for sensing applications. In the transmission-type SPR structure, propagating surface plasmons are outcoupled to radiation modes by dielectric and metallic gratings on a metal film. The results calculated in air and water suggest that the proposed structures present extremely linear sensing characteristics. In terms of a figure of merit, a metallic grating-based structure performs 5.4 and 3.7 times better than that of a dielectric grating in air and water, respectively.

OCIS codes: 050.2770, 230.1950, 240.6680.

1. Introduction

A surface plasmon is a quantum of an electron concentration wave that can exist at a dielectric–metal interface [1]. The surface plasmon propagates along the metal surface and decays exponentially into both media. When the momentum of an incident beam matches that of a surface plasmon, the beam energy is absorbed to excite surface plasmons. Since this resonance condition is sensitive to variations of the medium surrounding a metal surface, a small change in refractive index on a metal surface can be quantitatively analyzed by measuring the resonance shift in incidence angles or wavelengths. Surface plasmon resonance (SPR) is one of the well-known optical phenomena that have found useful applications in biochemical sensing [2]. Beginning with the pioneering work of Otto [3] and Kretschmann [4], SPR-based biosensors have been widely used as a sensitive probe to detect and analyze various biomolecular interactions on a metal surface.

Most plasmon-based biosensors work as reflection types in the sense that a photodetector measures reflected light at a metal by use of a standard Kretschmann configuration. Such a setup uses a photodetector on the same side of a light source with respect to the metal film, which allows an extremely compact biosensing scheme. On the other hand, an extinction-based transmission-type SPR biosensor is also plausible and has been extensively investigated to study spectral outcoupling of surface plasmons excited in nanostructures often using a wavelength-scanning setup [5,6]. Moreover, a transmission-type SPR structure might be useful to investigate thick targets such as in cell analysis, in contrast with a traditional reflection-type structure. Note that the detectable range of a reflection-type configuration is limited to the penetration depth in the 100–200 nm range, although this may be increased as a result of thin-film engineering [7]. The potential advantage of a transmission-type structure for investigation of a thick target is based on the excitation of radiation modes. Radiation modes can sense cell status variation by means of transmission or scattering, e.g., due to morphological changes of a cell. In the case of conventional reflection-type SPR sensors that do not outcouple a radiation mode, the detection range is intrinsically limited to the plasmon decay length into the surrounding liquid or gas.

0003-6935/07/235703-06$15.00/0

In other words, in a transmission-type SPR, excitation in radiation modes in addition to evanescent waves associated with plasmonic dipoles probes a target environment that consequently changes the radiation characteristics of transmitted light.

We theoretically investigate a grating-coupled transmission-type SPR sensor based on angle scanning, in which plasmon outcoupling into radiation modes is achieved by dielectric and metallic gratings on a metal film. Intriguing studies on outcoupling of excited surface plasmons with diffraction gratings have been carried out by many groups. Most of the early studies considered corrugated metallic gratings to excite surface plasmons and to outcouple them into radiation modes [8,9]. In actual applications that use outcoupled radiation, the converted propagating radiation has only reflection modes [10,11] that might not have enough power to associate them with other external optical devices. To overcome this limitation, Park *et al.* [12] utilized dielectric diffraction gratings for efficient outcoupling of surface plasmons to transmission modes. Use of a conventional Kretschmann configuration and dielectric gratings on a silver film, an outcoupling efficiency of 50% was presented and proved experimentally. From the report of Lenaerts *et al.* [13], transmittance of 68% was obtained for a modified structure in which a waveguide grating is added between a metal surface and air. Moreover, enhanced transmittance of up to 72% was predicted numerically by Shen *et al.* [14] with a brief report of its potential application as a biochemical sensor.

Our configuration employs a metallic grating that is introduced to convert surface plasmons into radiation modes. Compared with a dielectric grating, a metallic grating on a metal film could induce an increase of interaction area, which supports excitation of surface plasmons and mediates interaction between excited plasmons and local sensing events on a perturbed metal surface. A sharp transmission curve can also be produced from absorptive metallic gratings. The effect of a metallic grating will be discussed in detail later. We used rigorous coupled-wave analysis (RCWA) [15–17] to determine optimum dielectric and metallic grating structures and to compare transmission efficiency. This is then applied to biochemical sensing characteristics in air and water.

2. Numerical Model

Figure 1 shows a transmission-type SPR configuration with dielectric or metallic gratings. A 40 nm thick silver layer is deposited on a prism substrate and supports excitation of surface plasmons. One-dimensional diffraction gratings with a period Λ are regularly patterned on a metal film. The 300 nm wide grating structure has a period of $\Lambda = 600$ nm (i.e., $f = 50\%$). This is almost equal to the wavelength of an incidence beam ($\lambda = 633$ nm), so that only the low diffraction orders can transmit into air. The dielectric functions of a BK7 glass prism and gratings were determined, respectively, as $\varepsilon_p = 2.2958$ and $\varepsilon_g = 2.25$ [e.g., polymethyl methacrylate (PMMA)] [18] for a dielectric grating, and $\varepsilon_g = \varepsilon_m = -18 + 0.5i$ for silver at $\lambda = 633$ nm [11]. Here ε_m indicates metal permittivity.

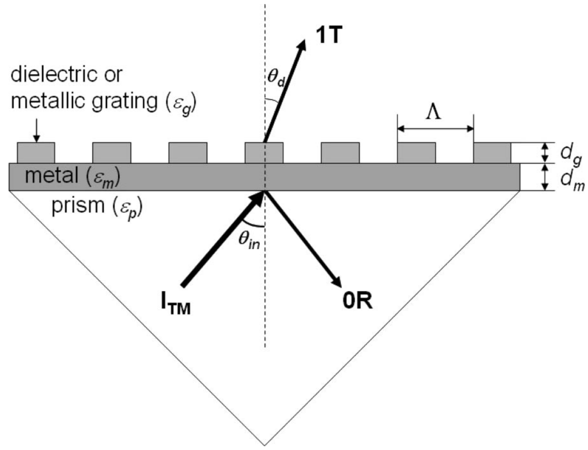

Fig. 1. Schematic diagram of a transmission-type SPR configuration with dielectric or metallic gratings. A thin metal film with a thickness of d_m is deposited on a prism substrate. Dielectric or metallic gratings with a period Λ and a fill factor f are regularly patterned on the metal layer. TM-polarized light is incident through the prism substrate at a fixed wavelength of $\lambda = 633$ nm. The diffracted light transmits into a superstrate environment (air or water).

When TM-polarized light is incident on a prism, the dispersion relation of the excited surface plasmons at resonance conditions is given by [1]

$$k_{\mathrm{SPR}} = k_0\left(\frac{\varepsilon_d\varepsilon_m}{\varepsilon_d + \varepsilon_m}\right)^{1/2} = \frac{w}{c}\sqrt{\varepsilon_p}\,\sin\theta_{\mathrm{SPR}}, \qquad (1)$$

where k_{SPR} and k_0 $(= w/c)$ denote the wave vectors of the surface plasmon and the incident light. Also, w is the angular frequency of the incident light, c is the speed of light in free space, θ_{SPR} is the incidence angle at resonance, and ε_d is the dielectric constant of the medium on top of a metal film. This relation indicates that a propagating surface plasmon along the metal surface is converted to a radiation mode by a diffraction grating when the diffracted angles satisfy momentum matching between surface plasmons and photons given by

$$k\,\sin\theta_d = k_{\mathrm{SPR}} - qK, \quad q = 0, \pm1, \pm2, \ldots, \qquad (2)$$

where k is the magnitude of the wave vector of the diffracted light, θ_d is the diffraction angle, q is the diffraction order, and K $(= 2\pi/\Lambda)$ is the grating vector. The first diffraction order (1T) has been selected as the target under interrogation instead of 0T, since 1T is the indicator of a radiation mode. The transmittance of the first-order diffraction mode is shown schematically in Fig. 1. An incident beam is TM polarized with a fixed wavelength of $\lambda = 633$ nm. The RCWA has been employed to analyze diffraction efficiencies of transmission modes. This algorithm has been successfully applied to explain the experimental results for periodic or aperiodic structures with a

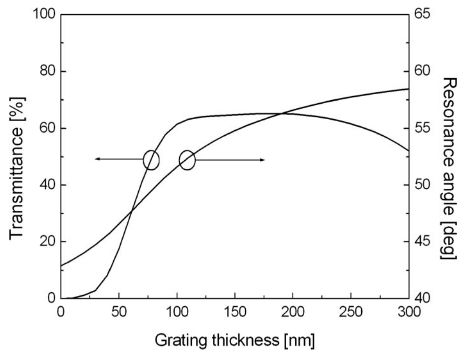

Fig. 2. Transmission characteristics of a transmission-type SPR structure with a dielectric grating. The effects of the grating thickness on the transmittance efficiency (1T) and the resonance angles are shown. The silver metal film thickness is $d_m = 40$ nm. The dielectric grating has a period of $\Lambda = 600$ nm and $f = 0.5$.

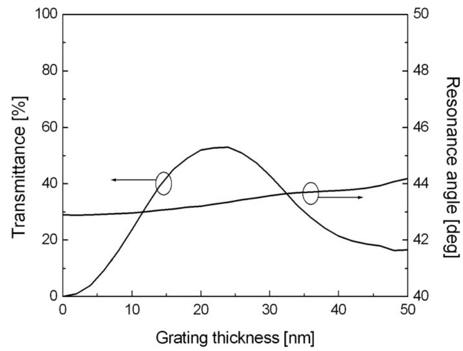

Fig. 4. Transmission characteristics of a transmission-type SPR structure with a metallic grating. The effects of the grating thickness on the transmittance efficiency (1T) and the resonance angles are shown. The silver metal film thickness is $d_m = 40$ nm. The silver metal grating has a period of $\Lambda = 600$ nm and $f = 0.5$.

dimension less than the wavelength of the incident light [19–21].

3. Results and Discussion

Figure 2 presents the transmittance and resonance angles of the first diffraction order (1T) for a dielectric grating-coupled SPR structure, as the grating thickness d_g varies from 0 to 300 nm. The transmittance and resonance characteristics exhibit strong dependence on the grating thickness. The transmittance rapidly increases first to 60% until d_g reaches 100 nm, and then it becomes nearly constant. As the thickness exceeds 250 nm, a slight decrease in transmittance appears since other diffraction orders become significant. High transmittance that exceeds 60% was obtained at a grating thickness in the 100–250 nm range with a maximum at $T_{\max} = 65.28\%$ at $d_g = 180$ nm. Also, the resonance angle increases monotonically with grating thickness as the change in d_g causes the local refractive index to increase effectively. The calculated reflection and transmission curves for the case of an optimal dielectric grating with peak transmittance are shown in Fig. 3. For sensitive detection of the transmitted light and its application as various optical devices, higher transmittance is desired. Maximum outcoupling of the propagating surface plasmons occurs at an incidence angle of $\theta_{\text{in}} = 55.92°$ with the full width at half-maximum (FWHM) of the transmission curve $\delta\theta_{\text{FWHM}} = \delta\theta_{\text{SPR}} = 3.12°$.

Figure 4 shows the transmittance and resonance characteristics of a metallic grating on a 40 nm silver surface. The peak efficiency obtained was $T_{\max} = 52.97\%$ at a thickness of $d_g = 24$ nm. In the range of $d_g > 50$ nm, the radiation modes are extinction dominated and largely attenuated because of the high absorption coefficient of silver, so that the transmittance is reduced to less than 20%. Also, when the grating thickness varies, the resonance angles increase slightly. The SPR curves at the peak transmittance found at an incidence of $\theta_{\text{in}} = 43.34°$ are shown in Fig. 5. Although a silver grating with high absorption can decrease the peak transmittance by more than 10% and induce a degradation of the whole radiation amplitude in comparison with a dielectric PMMA grating, the extremely narrow transmission peak calculated to be as small as 0.55° as shown in Fig. 5 can be an advantage of a metallic grating over a dielectric grating.

The proposed transmission-type SPR structure based on optimal dielectric and metallic gratings designed to provide maximum transmittance is now ap-

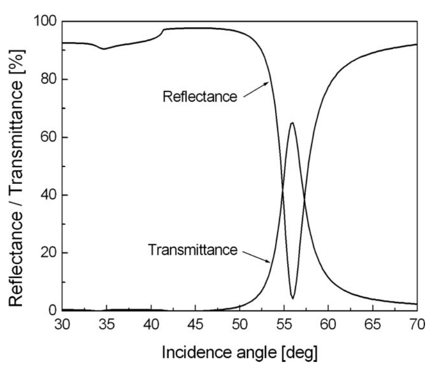

Fig. 3. Calculated reflectance and transmittance curves (1T) for a dielectric grating as a function of incidence angle. The grating thickness is $d_g = 180$ nm. At $\theta_{\text{in}} = 55.92°$, $T_{\max} = 65.28\%$.

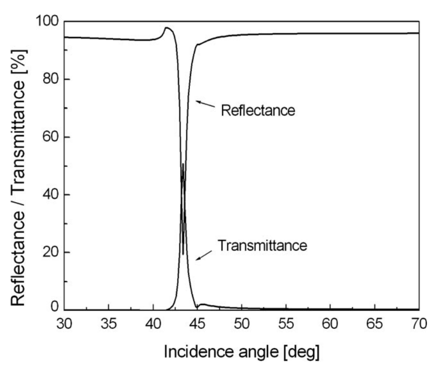

Fig. 5. Calculated reflectance and transmittance curves (1T) for a dielectric grating as a function of incidence angle. The grating thickness is $d_g = 24$ nm. At $\theta_{\text{in}} = 43.34°$, $T_{\max} = 52.97\%$.

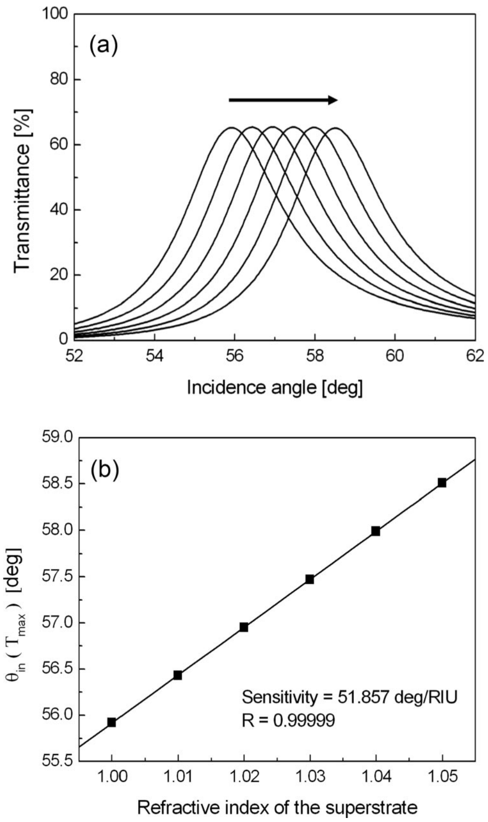

Fig. 6. (a) Transmittance and (b) linear regression analysis between resonance angle and superstrate refractive index of a transmission-type SPR sensor with a dielectric grating at d_g = 180 nm in air. As the refractive index of the superstrate increases from 1.00 to 1.05 in steps of 0.01, the transmittance peak shifts from 55.92° to 58.51° in the direction of the arrow. $\theta_{in}(T_{max})$ denotes the incidence angle at maximum transmittance.

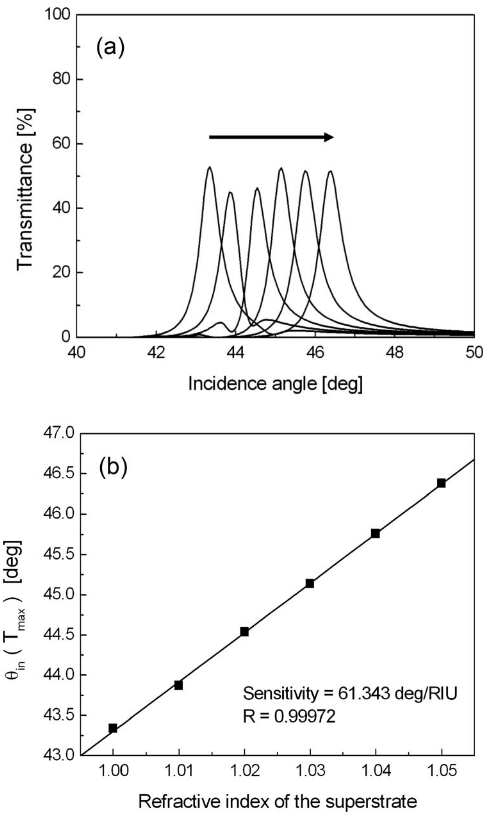

Fig. 7. (a) Transmittance and (b) linear regression analysis between resonance angle and superstrate refractive index of a transmission-type SPR sensor with a metallic grating at d_g = 24 nm in air. As the refractive index of the superstrate increases, the transmittance peak shifts from 43.34° to 46.38°.

plied as a biochemical sensor to detect gaseous and aqueous interactions. Considering that the resonance angle is sensitive to the local change in the environmental superstrate on the grating-metal film, the resonance angle shift and the diffraction efficiency are evaluated together as a function of the superstrate refractive index. Figure 6 shows that, for a dielectric grating, the resonance angle shifts from 55.92° to 58.51° as the refractive index of the superstrate varies from 1.00 to 1.05 in steps of 0.01. From linear regression analyses, the shift is completely linear over the whole range of refractive indices with $R = 0.99999$ (R is the correlation coefficient that denotes the linearity obtainable in the sensor performance) while the sensitivity, which indicates the slope of resonance angle over the refractive index, is 51.857 deg/refractive-index unit (RIU).

The influence of metallic gratings on the refractive-index sensitivity is shown in Fig. 7. Although the peak transmittance fluctuates because of the secondary sidelobes, silver gratings still support a high diffraction efficiency of greater than 40%. The resonance shift in response to an increase in the refractive index is extremely linear ($R = 0.99972$) with a sensitivity equal to 61.343 deg/RIU. In other words, a metallic grating shows an almost 20% greater sensitivity than a dielectric grating for the optimal configuration.

The plasmonic interpretation based on a surface-limited increase of interaction area and excitation of localized surface plasmons (LSPs) can be adopted to explain the enhanced sensitivity for a metallic grating. An increment of interaction area, induced by a metallic grating on a metal film, results in an additional resonance shift in response to the changes in local environments that surround the metallic surface. Moreover, enhanced fields from excited LSP modes can be attributed to the sensitivity enhancement. An incident beam and the propagating surface plasmons can directly interact through a metallic grating, which produces LSPs. The existence of a metallic grating near the metal film leads to a perturbation of the dispersion relation dictated by a conventional SPR structure and contributes to the sensitivity improvement by means of LSPs, although the LSP modes are not more dominantly excited than the propagating surface plasmons [22–24]. Furthermore, a sharp transmission peak is induced by the absorption property of silver metal gratings. The propagating surface plasmons are diffracted and pass through the absorptive metallic gratings, which prompts rapid attenuation of transmitted light. This effect is attributed to the narrow FWHM as well as the relative decrease in peak transmittance compared with that of dielectric diffraction gratings.

In addition to sensitivity, a figure of merit (FOM) [25] is introduced to effectively compare the overall performance of optical sensors as

$$\mathrm{FOM} = \frac{m(\mathrm{eV/RIU})}{\mathrm{FWHM(eV)}} T_{\max}, \tag{3}$$

where m is the slope of the resonance angle or resonance wavelength over the refractive-index range, which corresponds to the sensitivity of a SPR sensor. The FOM is equal to the quality factor that takes into account the transmittance for a transmission-type SPR structure. A smaller FWHM and a larger $T_{\max}$ are desired because a deeper and narrower resonance peak allows efficient detection of the resonance shift and precise analysis of sensing events. From our numerical results, FOM values were determined to be 10.85 for a dielectric grating and 59.08 for a metallic grating, respectively. Thus, a transmission-type SPR sensor with a metallic grating exhibits far better sensing performance by more than 5.4 times in comparison with a dielectric grating.

The proposed SPR structure can be applicable to detection in water. Efficient excitation of surface plasmons in water needs a high refractive-index prism substrate. The dielectric constants of a glass prism substrate and dielectric gratings were chosen to be $\varepsilon_p = 3.6639$ (e.g., SF66) and $\varepsilon_g = 3.88$ (e.g., ZrO_2) at $\lambda = 633$ nm. After a procedure identical to the case of a plasmon in air presented above, an optimal grating thickness was determined as $d_g = 80$ nm for a dielectric grating with $T_{\max} = 66\%$ at an incidence angle of $\theta_{\mathrm{in}} = 61.74°$. For a silver grating, the grating thickness was $d_g = 22$ nm with $T_{\max} = 40\%$ at $\theta_{\mathrm{in}} = 48.63°$.

If the dielectric grating is employed in biosensing applications, as the superstrate refractive index varies from 1.33 to 1.38 in steps of 0.01, the resonance angle shows a fairly linear shift ($R = 0.99993$) from 61.74° to 64.38° as shown in Fig. 8. The sensitivity was obtained as 52.686 deg/RIU with the FWHM of the transmittance curve at 6.24°. For a metallic grating, the sensitivity was 69.571 deg/RIU with $R = 0.99911$ and a FWHM of 1.35° as presented in Fig. 9. From these results, the FOM values were determined to be 5.57 for a dielectric grating and 20.61 for a metallic grating. A transmission-type SPR structure with a metallic grating also shows better performance by more than 3.7 times in comparison with a dielectric grating in water. Performance evaluation of a transmission-type SPR sensor for both air and wa-

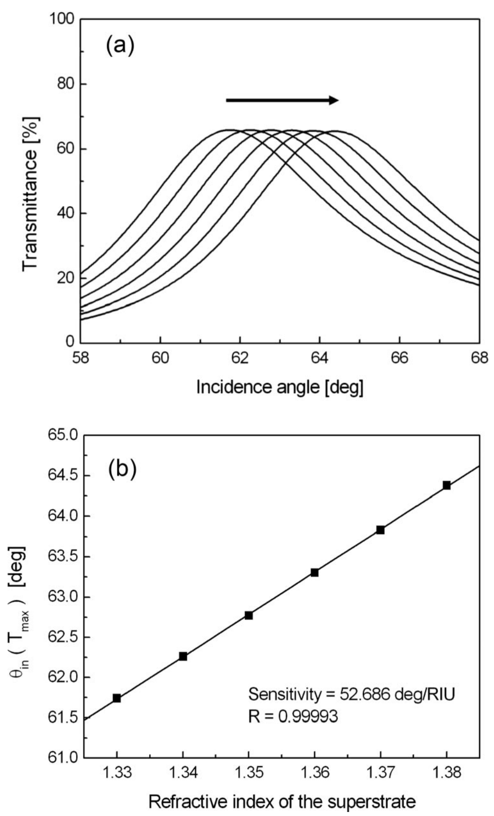

Fig. 8. (a) Transmittance and (b) linear regression analysis between resonance angle and superstrate refractive index of a transmission-type SPR sensor with a dielectric grating at $d_g = 80$ nm in water. As the refractive index of the superstrate increases from 1.33 to 1.38 in steps of 0.01, the transmittance peak shifts from 61.74° to 64.38° in the direction of the arrow.

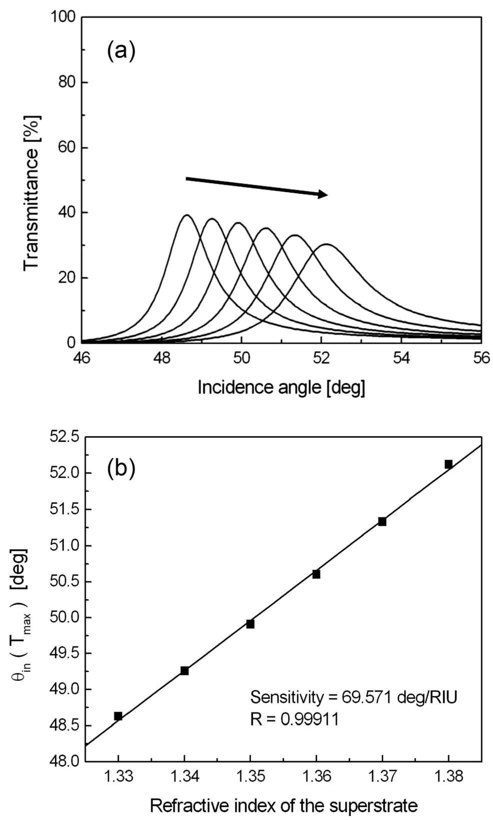

Fig. 9. (a) Transmittance and (b) linear regression analysis between resonance angle and superstrate refractive index of a transmission-type SPR sensor with a metallic grating at $d_g = 22$ nm in water. As the refractive index of the superstrate increases, the transmittance peak shifts from 48.63° to 52.12°.

ter suggests that a metallic grating-based structure outperforms that of a dielectric grating.

In terms of actual implementation, dielectric and metallic gratings on a silver film can be fabricated using electron-beam or interference lithography with a laser in the visible wavelength. A periodic grating structure with $\Lambda = 600$ nm can be achieved by plasma etching that follows deposition of a grating layer and lithography processes.

4. Conclusion

We have numerically investigated transmission-type SPR sensors with dielectric and metallic gratings. The transmission characteristics strongly depend on the grating material and thickness. Optimal grating thickness was determined in consideration of transmittance efficiency. In both air and water, a metallic grating-based structure presented higher sensitivity and a narrower FWHM despite lower maximum transmittance compared with a dielectric grating. For practical sensing applications, real-time detection of gaseous or aqueous changes can be accomplished by measuring the diffraction characteristics in an enhanced transmission mode. We have provided a feasible structure that can be used as a sensor and as other optical devices, for example, polarizer, filters, and modulators.

This research was supported by the Engineering Research Center program of the Ministry of Science and Technology/Korea Science and Engineering Foundation (KOSEF), R11-2000-075-01001-1. D. Kim acknowledges the support of the KOSEF through the National Core Research Center for Nanomedical Technology, R15-2004-024-00000-0, and by a Korea Research Foundation (KRF) grant funded by the Korean Ministry of Education and Human Resources Development under KRF-2005-205-D00051.

References

1. H. Raether, *Surface Plasmons on Smooth and Rough Surfaces and on Gratings, Springer Tracts in Modern Physics* (Springer-Verlag, 1988).
2. J. Homola, S. S. Yee, and G. Gauglitz, "Surface plasmon resonance sensors: review," Sens. Actuators B **54,** 3–15 (1999).
3. A. Otto, "Excitation of surface plasma waves in silver by the method of frustrated total reflection," Z. Phys. **216,** 398–410 (1968).
4. E. Kretschmann, "Decay of non radiative surface plasmons into light on rough silver films: comparison of experimental and theoretical results," Opt. Commun. **6,** 185–187 (1972).
5. A. J. Haes and R. P. Van Duyne, "A nanoscale optical biosensor: sensitivity and selectivity of an approach based on the localized surface plasmon resonance spectroscopy of triangular silver nanoparticles," J. Am. Chem. Soc. **124,** 10596–10604 (2002).
6. E. Hutter and J. H. Fendler, "Exploitation of localized surface plasmon resonance," Adv. Mater. **16,** 1685–1706 (2004).
7. S. J. Yoon and D. Kim, "Thin-film-based field penetration engineering for surface plasmon resonance biosensing," J. Opt. Soc. Am. A **24,** 2543–2549 (2007).
8. W. Rothballer, "The influence of surface plasma oscillations on the diffraction orders of sinusoidal surface gratings," Opt. Commun. **20,** 429–433 (1977).
9. N. Garcia, "Exact calculations of p-polarized electromagnetic fields incident on grating surfaces: surface polariton resonances," Opt. Commun. **45,** 307–310 (1983).
10. P. S. Vukusic, G. P. Bryan-Brown, and J. R. Sambles, "Surface plasmon resonance on gratings as a novel means for gas sensing," Sens. Actuators B **8,** 155–160 (1992).
11. M. J. Jory, P. S. Vukusic, and J. R. Sambles, "Development of a prototype gas sensor using surface plasmon resonance on gratings," Sens. Actuators B **17,** 203–209 (1994).
12. S. Park, G. Lee, S. H. Song, C. H. Oh, and P. S. Kim, "Resonant coupling of surface plasmons to radiation modes by use of dielectric gratings," Opt. Lett. **28,** 1870–1872 (2003).
13. C. Lenaerts, F. Michel, B. Tilkens, Y. Lion, and Y. Renotte, "High transmission efficiency for surface plasmon resonance by use of a dielectric grating," Appl. Opt. **44,** 6017–6022 (2005).
14. S. Shen, E. Forsberg, Z. Han, and S. He, "Strong resonant coupling of surface plasmon polaritons to radiation modes through a thin metal slab with dielectric gratings," J. Opt. Soc. Am. A **24,** 225–230 (2007).
15. M. G. Moharam and T. K. Gaylord, "Diffraction analysis of dielectric surface-relief gratings," J. Opt. Soc. Am. **72,** 1385–1392 (1982).
16. M. G. Moharam and T. K. Gaylord, "Rigorous coupled-wave analysis of metallic surface-relief gratings," J. Opt. Soc. Am. A **3,** 1780–1787 (1986).
17. L. Li and C. W. Haggans, "Convergence of the coupled-wave method for metallic lamellar diffraction gratings," J. Opt. Soc. Am. A **10,** 1184–1189 (1993).
18. Y.-J. Hung, I. I. Smolyaninov, Q. Balzano, and C. C. Davis, "Strong optical coupling effects through a continuous metal film with a surface dielectric grating," in *Plasmonics: Metallic Nanostructures and Their Optical Properties III,* M. I. Stockman, ed., Proc. SPIE **5927,** 386–394 (2005).
19. J. Lermé, "Introduction of quantum finite-size effects in the Mie's theory for a multilayered metal sphere in the dipolar approximation: application to free and matrix-embedded noble metal clusters," Eur. Phys. J. D **10,** 265–277 (2000).
20. E. Moreno, D. Erni, C. Hafner, and R. Vahldieck, "Multiple multipole method with automatic multipole setting applied to the simulation of surface plasmons in metallic nanostructures," J. Opt. Soc. Am. A **19,** 101–111 (2002).
21. J. Cesario, R. Quidant, G. Badenes, and S. Enoch, "Electromagnetic coupling between a metal nanoparticle grating and a metallic surface," Opt. Lett. **30,** 3404–3406 (2005).
22. K. M. Byun, S. J. Kim, and D. Kim, "Design study of highly sensitive nanowire-enhanced surface plasmon resonance biosensors using rigorous coupled wave analysis," Opt. Express **13,** 3737–3742 (2005).
23. K. M. Byun, D. Kim, and S. J. Kim, "Investigation of the profile effect on the sensitivity enhancement of nanowire-mediated localized surface plasmon resonance biosensors," Sens. Actuators B **117,** 401–407 (2006).
24. D. Kim, "Effect of resonant localized plasmon coupling on the sensitivity enhancement of nanowire-based surface plasmon resonance biosensors," J. Opt. Soc. Am. A **23,** 2307–2314 (2006).
25. L. J. Sherry, S.-H. Chang, G. C. Schatz, R. P. Van Duyne, B. J. Wiley, and Y. Xia, "Localized surface plasmon resonance spectroscopy of single silver nanocubes," Nano Lett. **5,** 2034–2038 (2005).